

The Arctic and Antarctic Oscillations in the IPCC AR4 Coupled Models*

ZHU Yali^{1,2,3†}(祝亚丽) and WANG Huijun^{1,3}(王会军)

¹ Nansen-Zhu International Research Center, Institute of Atmospheric Physics, Chinese Academy of Sciences, Beijing 100029

² Graduate School of Chinese Academy of Sciences, Beijing 100049

³ Climate Change Research Centre, Chinese Academy of Sciences, Beijing 100029

(Received March 24, 2009)

ABSTRACT

This study evaluates the fidelity of Arctic and Antarctic oscillations (AO and AAO for short, respectively) in the coupled general circulation models participating in the Fourth Assessment Report of Intergovernmental Panel on Climate Change (IPCC AR4). The AO and AAO during 1970–1999 in 24 models are analyzed and compared with that in ERA-40 and NCEP-1. Models' performance is seasonally dependent, with best reproducibility of both spatial structure and trend in winter. In most models, the spatial pattern and temporal trend of AAO during this period are more delicately simulated than AO. After picking out models with better performance according to the Taylor diagram, we find that their ensemble mean can obviously improve models' reproducibility. The AO and AAO in the Special Report on Emission Scenarios (SRES) A1B Projection during the 21st century are also briefly analyzed. The results reveal that both the AO and AAO indices keep increasing during 1970–2099, with a steadier pace of AO than AAO. The spatial difference of sea level pressure between 2060–2089 and 1970–1999 shows decreased values in polar regions, and increased values in midlatitudes. The results manifest that the ozone recovery during the mid 21st century may not weaken such a trend.

Key words: Antarctic oscillation, Arctic oscillation, IPCC, coupled model, annular mode

Citation: Zhu Yali and Wang Huijun, 2010: The Arctic and Antarctic oscillations in the IPCC AR4 coupled models. *Acta Meteor. Sinica*, **24**(2), 176–188.

1. Introduction

There exists a strong leading mode in the anomalous sea level pressure (SLP) field of the mid-high latitudes in both hemispheres at various time scales, i.e., synoptic, monthly, seasonal, and interannual. This mode is shown as a seesaw between the anomalous SLP in the polar region and midlatitudes, namely, decreased polar low often accompanies increased mid-latitude high, and vice versa. It corresponds to the out-of-phase relation between the zonal wind anomalies along 40°N and 60°N. Thus, this mode is named the Arctic/Antarctic oscillation (AO/AAO, or the northern/southern annular mode due to their zonally symmetric structure) in the Northern/Southern Hemisphere. The AO/AAO can be represented by the first leading mode of the empirical orthogonal function

(EOF) analysis on the SLP field north of 20°N (south of 20°S). And vertically, the AO/AAO is equivalent barotropic, as the seesaw structure exists in the entire troposphere, and the amplitude increases with height (Thompson and Wallace, 1998, 2000a; Gong, 1998). The AO/AAO is produced by the internal variability of the atmosphere with no major period. Many studies investigate the mechanism how the related zonal wind anomalies persist, and Lorenz and Hartmann (2001, 2003) found that the major contribution comes from the interaction between the zonal-mean wind anomalies and the baroclinic transient waves.

As a hemispheric-scale atmospheric mode, AO/AAO can exert significant impacts on the weather and climate systems in many regions. AO can influence the surface temperature of East Asia in winter through the Siberian high (Gong et al., 2001); positive

*Supported by the National Natural Science Foundation of China under Grant Nos. 40523001 and 40631005, and Chinese Academy of Sciences under Grant Nos. KZCX2-YW-Q1-02 and KZCX2-YW-Q11-05.

†Corresponding author: zhuyli@mail.iap.ac.cn.

(Chinese version published in Vol. 66, No. 6, 2008)

AO in late spring will induce the northward shift of the East Asian jet in summer, less rainfall in the Yangtze River and South Japan, and more rainfall in South China (Gong and Ho, 2003); winter AO can modulate the precipitation in Southeast Africa through the impact on the shift of the intertropical convergence zone (McHugh and Rogers, 2001). Thompson and Wallace (2001) made a comprehensive study on the regional climate impact of AO and found that AO can modulate the intensity of the midlatitude storms, the frequency of the blocking high and the cold air outbreak in the high latitudes. AAO can influence the precipitation variability in many regions in the southern high latitudes (Gillett et al., 2006). AAO exerts an impact on the winter-spring climate and summer rainfall in East Asia through the atmospheric circulation (Wang and Fan, 2005; Fan and Wang, 2006). The moisture budget related to AO/AAO is also zonally symmetric: when the polar low deepens, the associated westerly anomalies and meridional thermodynamical circulation can induce moisture divergence and decrease the precipitation (Boer et al., 2001).

During recent decades, AO/AAO index shows an obvious upward trend. And this trend results from the interactions among several factors including the global warming, stratosphere ozone depletion, and sea-ice attenuation (Arblaster and Meehl, 2006; Thompson et al., 2000b). The AO/AAO not only modulates the global climate at the interannual time scale, but also the global climate change at multi-decadal or even longer time scales. In the 1980s and 1990s, strengthened AO induces decreased SLP in the polar region and anomalous cyclonic motion of sea ice, and thus the contraction of the Eurasian ice (Hu et al., 2002; Rigor et al., 2002). The changing pattern of the Northern Hemisphere surface air temperature resembles the spatial pattern of AO from the 1970s to the end of 20th century (Thompson and Wallace, 1998). The strengthened AAO makes the Antarctic continent somewhat isolated from the global warming, while there exists above-global-mean temperature rise in the Antarctic Peninsula (Marshall, 2007). Thompson and Solomon (2002) showed that the strengthened AAO intensifies the westerly flow encircling the polar cap and results in the warming over the Antarctic

Peninsula and the cooling over eastern Antarctica and the Antarctic Plateau.

Due to the significant regional and remote influences of AO/AAO mentioned above, their changes have significant implications for climate change in many regions over the earth. In addition, as the major atmospheric circulation modes in the mid-high latitudes, it is rather important to know how well the coupled models can reproduce the spatial and temporal characteristics of AO/AAO. In this paper, we try to evaluate the capability of the coupled general circulation models from IPCC AR4 (the Fourth Assessment of the Intergovernmental Panel on Climate Change) in reproducing AO/AAO, including the spatial pattern, trend and interannual variability, and to reveal the future changes of AO/AAO so as to provide some clues for global, especially high latitude, climate change. The details on why some models exhibit good reproducibility while others are poor will not be involved too much in this study.

2. Models and methods

The SLP of the coupled models is retrieved from the Program of Climate Model Diagnosis and Intercomparison at the website: <http://www-pcmdi.llnl.gov/>. Table 1 lists the brief information of these models, and details can also be found in the above website. The 20C3M simulates the 20th century climate (starting from the mid-19th century). There are three simulations for the future climate based on the emission scenarios of the IPCC Special Report on Emission Scenarios (SRES): SRES-A1B, SRES-A2, and SRES-B1. The output data of 24 models for 20C3M and SRES-A1B are utilized in this study.

The models have one to nine experiment members. The giss-aom, ipsl-cm4, ukmo-hadcm3, and ukmo-hadgem are experimented with two runs; gfdl-cm2.0, gfdl-cm2.1, iap-fgoals1.0-g, and micro3.2-medres with three; bcc-cm1, mpi-echam5, and ncar-pcm1 with four; cccma-cgcm3.1-t47, giss-model-eh, miub-echo-g, and mri-cgcm2.3.2a with five; ncar-ccsm3.0 with eight; and giss-model-e-r with nine; and the rest seven models with only one. We first calculated the multi-run mean SLP field of each model, and

Table 1. Information on models participating in the CMIP3

Code	Model Name	Institute	Number of runs (20C3M)	Atmospheric resolution	Stratosphere ozone
a	ncep				
b	ensemble				
c	bccr_bcm2_0	Bjerknes Center for Climate Research, Norway	1	T63, L31	×
d	cccma_cgcm3_1_t47	Canadian Centre for Climate Modelling and Analysis, Canada	5	3.75*3.75, L31	×
e	cccma_cgcm3_1_t63	**	1	2.8×2.8, L31	×
f	cnrm_cm3	Center National de Recherches Meteorologiques, France	1	T63, L45	✓
g	csiro_mk3_0	Commonwealth Scientific and Industrial Research Organisation, Australia	3	T63, L18	✓
h	csiro_mk3_5	**	1	**	✓
i	gfdl_cm2_0	Geophysical Fluid Dynamics Laboratory, NOAA, USA	3	2.5×2.0, L24	✓
j	gfdl_cm2_1	**	3	**	✓
k	giss_aom	NASA/Goddard Institute for Space Studies (GISS), USA	2	4×3, L12	×
l	giss_model_e_h	**	5	5×4, L20	✓
m	giss_model_e_r	**	9	**	✓
n	iap_fgoals1_0_g	Institute of Atmospheric Physics, China	3	2.8×2.8, L26	×
o	ingv_echam4	Istituto Nazionale di Geofisica e Vulcanologia, Italy	1	T106, L19	×
p	inmcm3_0	Institute for Numerical Mathematics, Russian Academy of Sciences, Russia	1	5×4, L21	×
q	ipsl_cm4	Institut Pierre Simon Laplace, CNRS CEA, France	2	3.75×2.75, L19	×
r	miroc3_2_hires	Center for Climate System Research (CCSR/NIES/FRCGC), Japan	1	T106, L56	✓
s	miroc3_2_medres	**	3	T42, L20	✓
t	miub_echo_g	Meteorological Institute of the University of Bonn/Institute of KMA, Germany&Korea	5	T30,L19	×
u	mpi_echam5	Max Planck Institute for Meteorology, Germany	4	T63, L31	✓
v	mri_cgcm2_3_2a	Meteorological Research Institute, Japan Meteorological Agency, Japan	5	T42, L30	×
w	ncar_ccsm3_0	National Center for Atmospheric Research, NSF/DOE/NASA/NOAA, USA	8	T85, L26	✓
x	ncar_pcm1	**	4	T42, L26	✓
y	ukmo_hadcm3	Hadley Centre for Climate Prediction and Research, Met Office, U.K.	2	3.75×2.75, L19	✓
z	ukmo_hadgem1	**	2	N96, L38	✓

Note: ** Same as the last model in the table.

“✓” and “×” denote models with stratosphere ozone depletion and recovery and models with only climatological ozone.

then applied EOF analysis on the SLP over south of 20°S and north of 20°N to obtain the AAO and AO mode. The inter-member standard deviation indicates model's internal variability, which can be reduced to

some extent through the multi-member-mean method. The spatial pattern of multi-model-ensemble (MME) is represented by the leading EOF of the averaged SLP. In order to separate the influence of ozone change on

the trend of AAO and AO, models are divided into two groups: the first group with stratospheric ozone depletion in 20C3M and ozone recovery in SRES A1B, the second with just climatological ozone. The MME of the two groups is abbreviated as MME-ozone and MME-nozone.

As pointed out by Marshall (2003), the calculated trends of AAO with NCEP/NCAR reanalysis are exaggerated by a factor of 2, while ERA-40 provides an improved representation of the Southern Hemisphere high-latitude circulation. Thus we use the SLP of both ERA (European Center for Medium-Range Weather Forecast) reanalysis (ERA-40) and NCEP/NCAR (National Centers for Environmental Prediction/National Center of Atmospheric Research) reanalysis 1 data to evaluate the models' reproducibility in terms of AAO and AO. The period of 1970–1999 is selected. The four seasons are defined as winter (December–January–February), spring (March–April–May), summer (June–July–August), and autumn (September–October–November).

3. Reproducibility of the IPCC AR4 coupled models on AAO

3.1 Spatial structure

The correlation coefficient between the spatial pattern of AO/AAO in the model and in ERA depicts the models' ability to capture the location of major centers. The root mean square difference shows the similarity of the modeled pattern with that in ERA (the closer to zero, the better), and the standard deviation indicates the models' capability to reproduce the amplitude. The above three variables shown together in one single diagram (Taylor diagram) can fully and clearly manifest the model's reproducibility (Taylor, 2001). The Taylor diagram of seasonal spatial AAO shows a higher correlation coefficient and a closer to zero root mean square difference of the models in winter in contrast to other seasons (figure omitted), indicating that the models' reproducibility are seasonally dependent, with best performance in winter. Thus, detailed results in winter are shown in the following

text.

Figure 1 shows the correlation coefficient, root mean square difference, and standard deviation of all models' spatial pattern and their ensembles relative to that of ERA (the reference point with standard deviation and correlation coefficient of 1.0) in winter. We obtain Figs. 1a and 1b based on the computation using each model's all members and only the first member, respectively. Obviously, the all-member-ensemble shows an overall smaller standard deviation than reanalysis due to the counterbalance among different members. This is even more evident for models with more members, e.g., giss-model-e-r with nine runs and ncar-ccsm3.0 with eight, which manifests that though the ensemble mean can reduce to some extent model's internal variability, it also weakens model's signals. In addition, models have different number of members in 20C3M and SRES A1B. Thus, to insure the uniformity of results, only the first member of each model is used in the following analysis.

In winter, the explained variance by AAO is 42.5% and 43.7% in ERA and NCEP, and the models resolve the AAO pattern with percentage variance explained from 26.6% to 73.3%. The main feature of AAO is the zonal wave-3 pattern with three positive centers over the midlatitude ocean, and one negative center over the polar region with a cyclonic center between 0° and 90°W (Raphael and Holland, 2006), which is highly consistent between ERA and NCEP (Figs. 2a, b). All models can reproduce the negative values over Antarctic and the positive belt over the midlatitudes, and the major difference exists in the intensity and position of the active centers. The MME pattern (Fig. 2c) also shows the zonal wave-3 pattern, but the amplitude is too weak to represent the real state, which can be attributed to the large inter-model discrepancies, and the Atlantic center is positioned too westward. Thus, model evaluation and selection should be performed.

According to the Taylor diagram, 10 models are selected: bccr-bcm2.0, cnrm-cm3, giss-model-e-h, giss-model-e-r, iap-fgoals1.0-g, miroc3.2-hires, mpi-echam5, mri-cgcm2.3.2a, ukmo-hadcm3, and ukmo-hadgem1, all with the root mean square difference

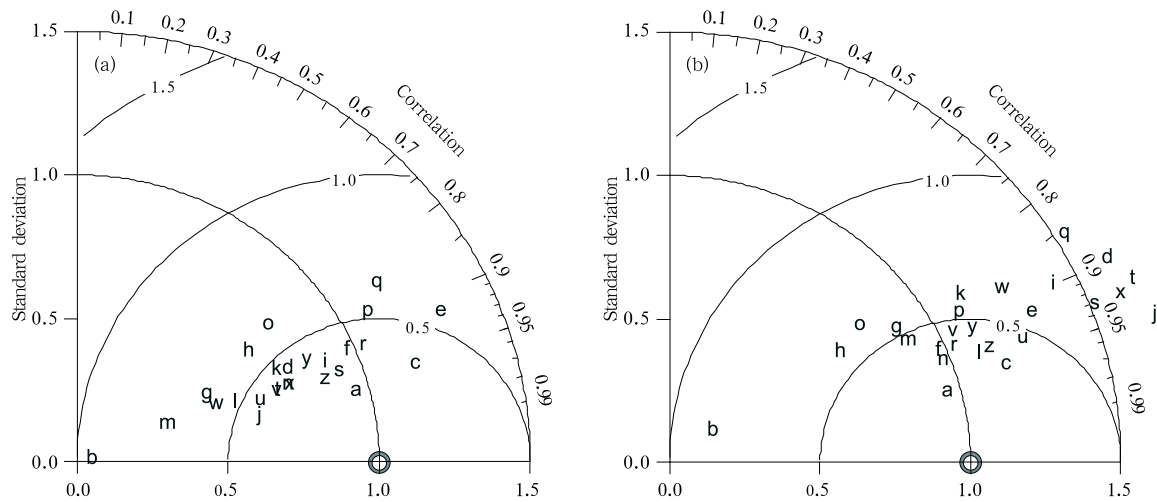


Fig. 1. Taylor diagrams of the spatial pattern of AAO with (a) multi-member-ensemble mean and (b) only the first run of individual models. The circle denotes the reference point—the observed AAO pattern in the ERA data. The radial distance of model code point from the origin is proportional to the standard deviation of the modeled AAO pattern relative to the observed AAO pattern of the ERA. The correlation coefficient between the model's pattern and the ERA pattern is shown by the cosine of the azimuthal angle of model code point, and their root mean square difference is given by the distance of model code point from the reference point.

less than 0.5, standard deviation larger than 1/4 but less than that of ERA, and correlation coefficient higher than 0.85. A point should be made clear that though these models show a delicate AAO spatial structure, large discrepancies occur between them in the future spatial pattern, and the model mpi-echam5 shows a quite different pattern among them during 2060–2089, thus it is better not to use this model's results to compute the ensemble mean of selected models. The ensemble mean of the nine models (Fig. 2d) more realistically depicts the spatial structure of AAO, with a higher correlation coefficient of 0.96, closer standard deviation of 1.01, and smaller root mean square difference of 0.31 relative to ERA.

Although the nine models are selected as the best ones, discrepancies with the reanalysis occur in many details. Miroc3.2-hires simulates a weaker center over the Indian Ocean, which is stronger in ukmo-hadcm3 and ukmo-hadgem1; the Pacific center is positioned somewhat more westward in most models; the Atlantic center is not shown in bccr-bcm2.0, cnrm-cm3, and mri-cgcm2.3.2a, and positioned too westward in ukmo-hadcm3; ukmo-hadgem1 produces a wave-4 pattern, with a pseudo center over the Southeast Pacific comparable to that over the Southwest Pacific. With

respect to the cyclonic center west of the Antarctic Peninsula, two models, mri-cgcm2.3.2a and had-cm3, show the center with equivalent amplitude at a location close to that in ERA.

Two couples of models are compared, respectively: cccma-cgcm3.1-t63 and cccma-cgcm3.1-t47, miroc3.2-hires and miroc3.2-medres, with the same model components and coupled details, just with a higher resolution in the former one. The models cccma-cgcm3.1-t63 and miroc3.2-hires show standard deviation closer to that of ERA, implying that with the same physical processes, models with higher resolution favor more realistic spatial pattern. On the other hand, however, giss-model-e-h and giss-model-e-r, which have the lowest resolution among all the models, still simulate the best spatial pattern. Thus, reasonable physical processes are vital for models' performance, while higher resolution can somewhat refine their performance.

3.2 Trend and interannual variability

Figure 3a shows the trend of AAO index in ERA, NCEP, MME, MME-ozone, MME-nozone, and 24 models. The AAO indices in both ERA and NCEP exhibit strong positive trends (significant at the 95%

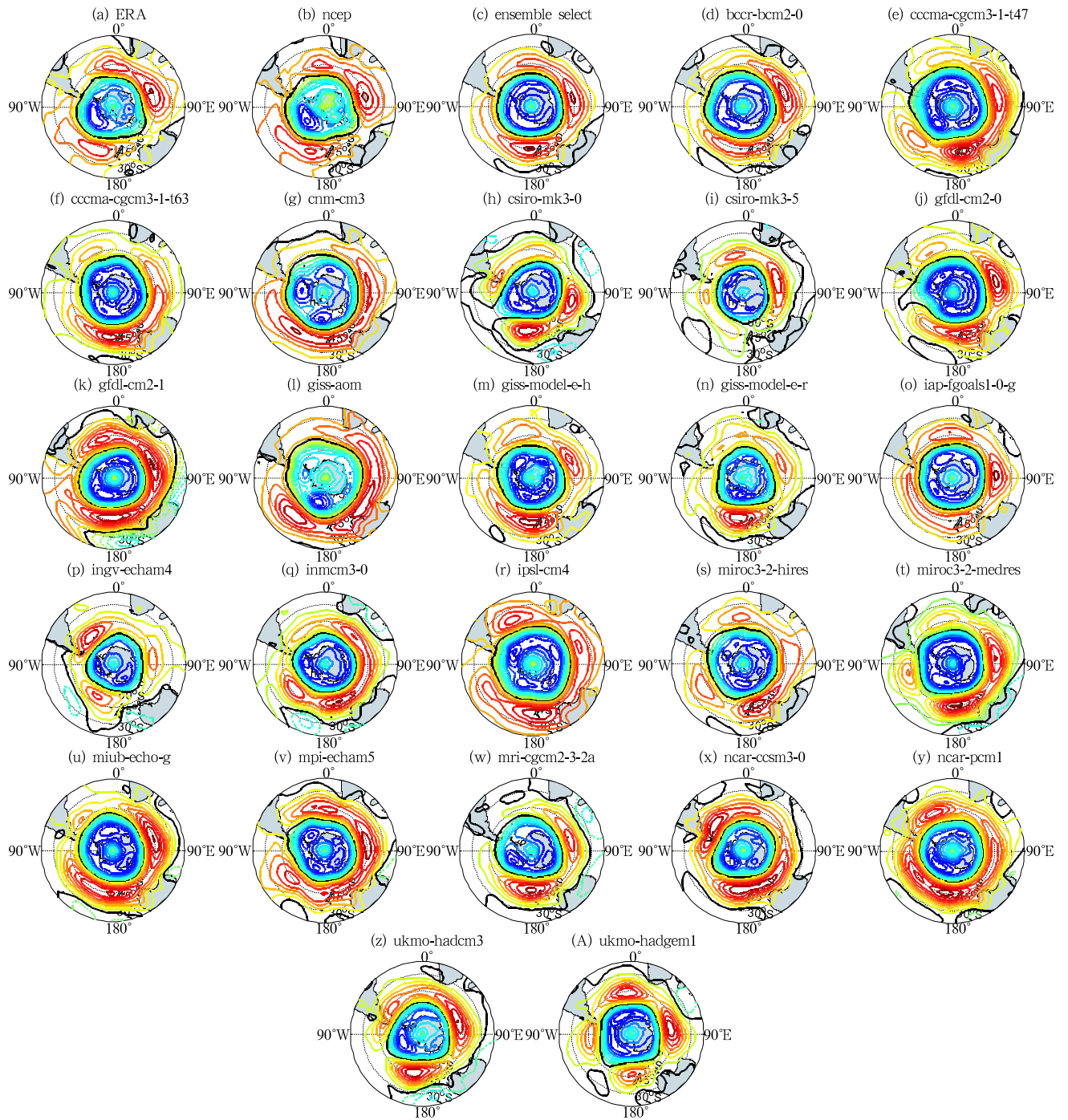


Fig. 2. Spatial patterns of AAO during 1970–1999 from (a) the ERA-40 reanalysis data, (b) the NCEP/NCAR reanalysis 1 data, (c) the ensemble mean of nine selected models, and (d)–(A) each of the 24 models.

confidence level) in winter and spring, significant and insignificant (at the 90% confidence level) positive trends in autumn and summer, respectively. These characteristics are consistent with the findings of Mar-

shall (2003) using station data—the strongest seasonal trend of AAO appears in austral summer.

Most models underestimate the seasonal trend. For example, all three ensembles exhibit much weaker

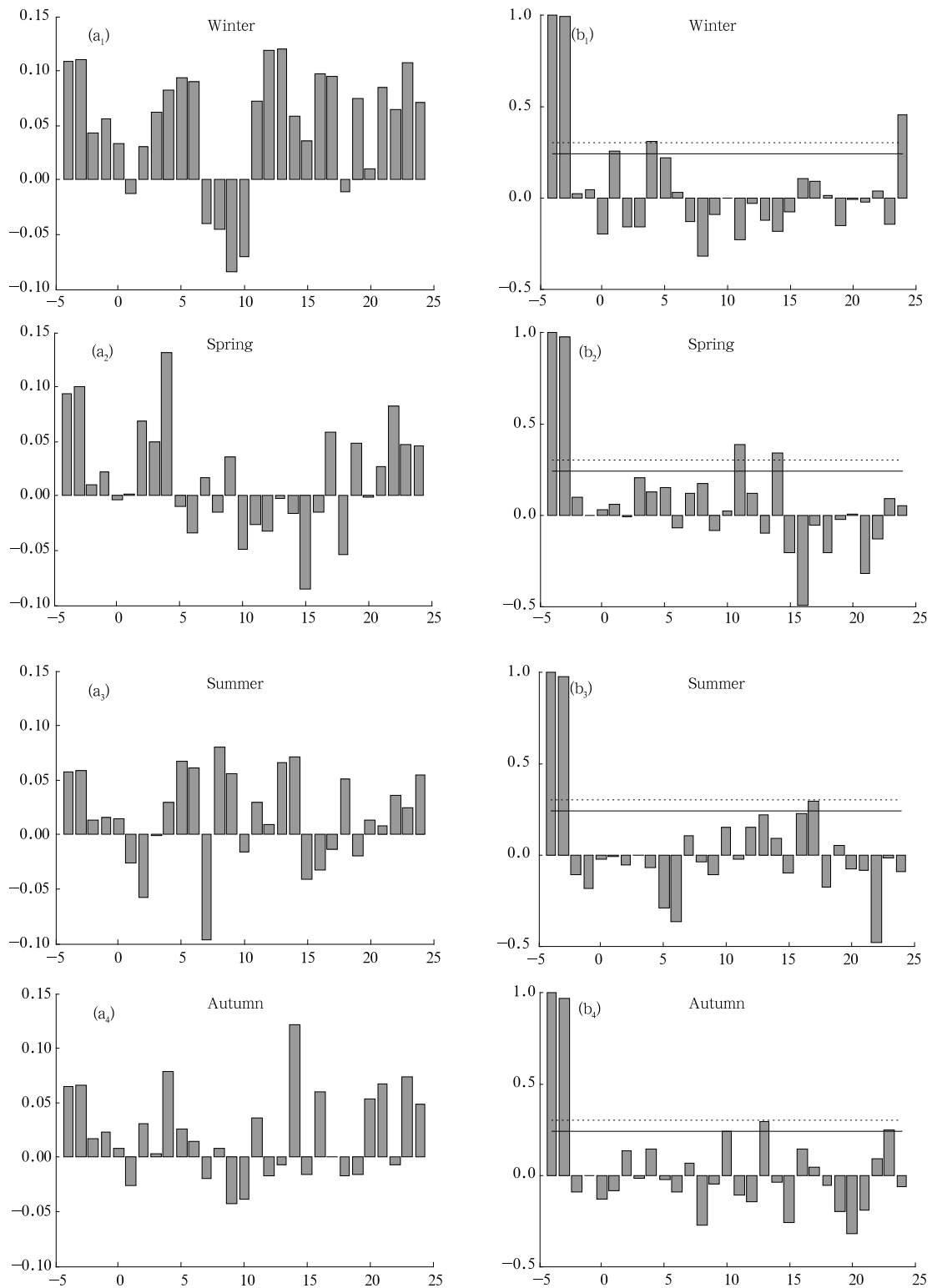


Fig. 3. Trends of (a) AAO index and (b) correlation coefficients between AAO index in models and ERA in the four seasons (denoted by subscripts 1-4) during 1970-1999. Numbers in the abscissa: -4 to 0 are ERA, NCEP, MME, MME-ozone, and MME-nozone, respectively, and 1 to 24 denote individual model following the order in Table 1.

trends than reanalysis; even MME-ozone has just a little more than half of the amplitude of the “realistic” trend. This is somewhat inconsistent with the conclusion of Cai and Cowan (2007), who showed that the AR4 model ensemble with ozone-depletion produces a comparable trend of the Southern Hemisphere circulation to the observation-corrected NCEP data. MME-ozone/MME-nozone shows a stronger/weaker trend than that of MME, respectively, and their difference suggests that ozone depletion contributes at least one third of the total AAO trend. Among the 24 models, 14 have realistic ozone depletion for 20C3M, four of which (ncar-pcm1, gfdl-cm2.0, gfdl-cm2.1, and giss-model-e-h) show insignificant even negative trends, others producing significant but weaker than realistic positive trends. Among the models with only climatological ozone, two models (iap-fgoals1.0-g and ingv-echam4) show trends equivalent to ERA and with the largest magnitude among all the models; others show insignificant or negative trends.

In winter, 10 models with stratospheric ozone depletion (cnrm-cm3, csiro-mk3.0, csiro-mk3.5, giss-model-e-r, miroc3.2-medres, miroc3.2-hires, mpi-echam5, ncar-ccsm3.0, ukmo-hadcm3, and ukmo-hadgem1) simulate significant (at the 90% confidence level) positive trends in AAO. In spring, cnrm-cm3 and ncar-pcm1 perform better than other models. Cnrm-cm3 is the only model that successfully shows the significant positive AAO trends in winter, spring, and autumn.

All indices are detrended first before calculating the correlation coefficient between the indices of models and ERA. AAO indices from ERA and NCEP are consistent at interannual time scale in four seasons, with correlation coefficients all above 0.9. As a whole, the models show very low capability to capture the realistic interannual variability of AAO (Fig. 3b). Three models (bccr-bcm2.0, cnrm-cm3, and ukmo-hadgem1) in winter produce interannual AAO indices significantly correlated (at the 80% confidence level) with that of ERA. The interannual variability mainly comes from the internal signal of atmosphere, and it proves quite a tough task for models to capture the natural variability of the atmosphere.

4. Reproducibility of models on AO

As the leading EOF mode, AO in winter can explain 36.1% and 34.2% variance in ERA and NCEP, and the explained variance is 32.2% in the MME, ranging from 23.1% to 42.2% in other models. Compared with AAO, the models exhibit weaker reproducibility of the spatial structure of AO, with smaller correlation coefficients in all four seasons (Fig. 4a). Models show a great scatter in the Taylor diagram, manifesting the large discrepancies. In winter, 16 models produce much stronger Pacific center, and the MME even cannot capture the major centers of AO (figure omitted), indicating the great inter-model discrepancies again. Thus, we select several models with better behavior according to the Taylor diagram and the models’ spatial structure. Eight models (cccma_cgcm_3.1_t47, cccma_cgcm_3.1_t63, gfdl_cm_2.0, giss-aom, miroc3.2-medres, ncar-pcm1, ukmo-hadcm3, and ukmo-hadgem1) are selected.

The spatial structure of AO in ERA and NCEP also shows great consistency (Figs. 5a, b), with an anomalous low pressure center occupying the Arctic region, and a weaker high pressure center over the mid-high latitude Pacific, and a stronger one over the East Atlantic to Scandinavia. Results of individual models are shown in Figs. 5d–A. Eight models resolve the positive centers over Pacific and Atlantic at the “almost right” position, while other models show obvious departure from the realistic location of the two centers. The ensemble-average of the eight models (Fig. 5c) describes the Pacific, Atlantic, and Arctic centers at equivalent location, but with much weaker Atlantic and Arctic centers, and a stronger Pacific center.

Both ERA and NCEP show a significant (at the 90% confidence level) positive trends of AO in winter and insignificant trend in other seasons (Fig. 4 b). The comparable positive trend in winter is manifested only in cnrm-cm3 and ncar-pcm1, which confirms the point made by Moritz et al. (2002) that most simulations show a much weaker AO trend than observations. Trends in MME-ozone and MME-nozone show no obvious difference, implying that the contribution of ozone depletion to this trend is weak. Models’ low reproducibility in the winter trend probably indicates the complex causes of AO change, including

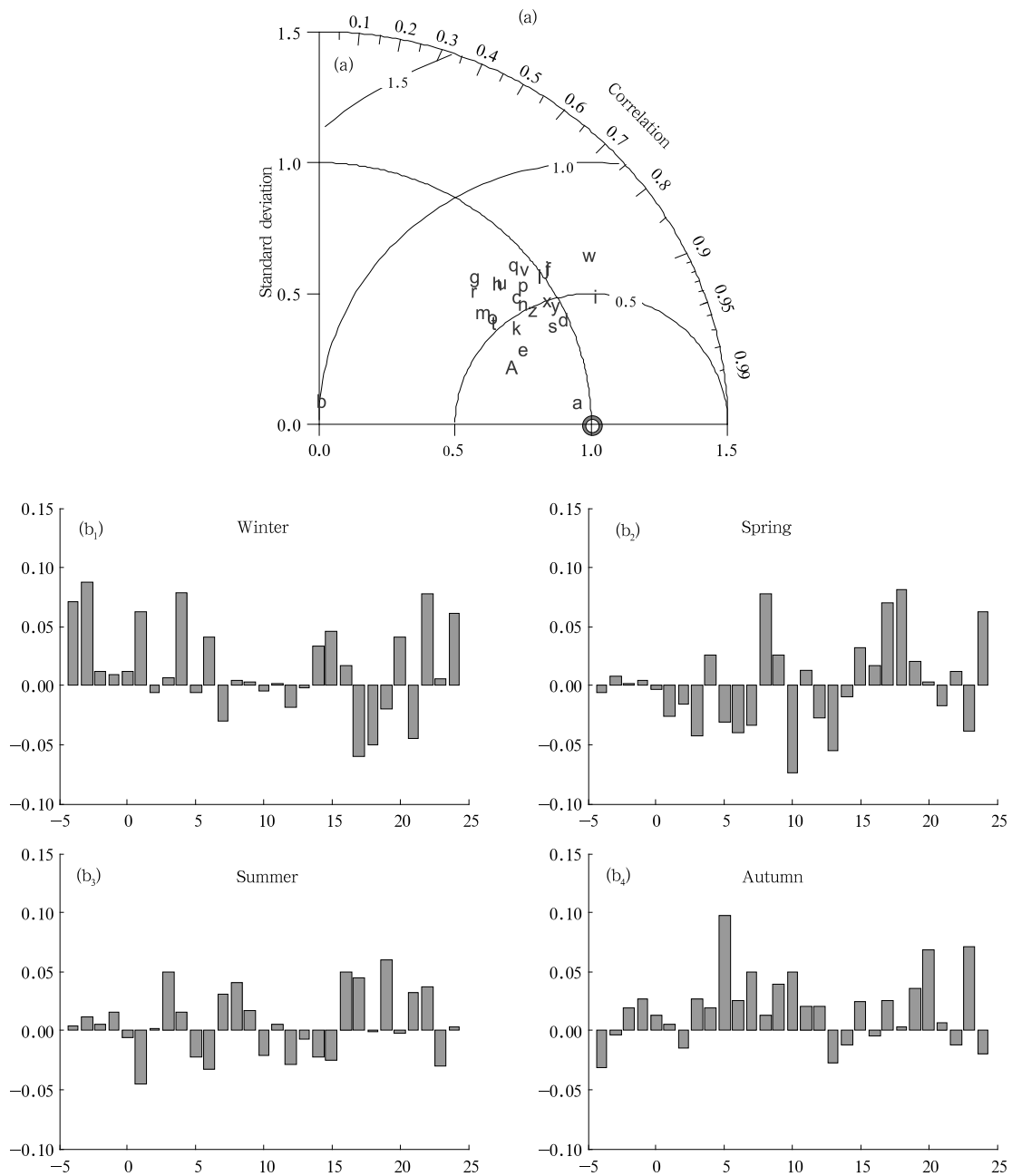


Fig. 4. (a) As in Fig. 1, but for AO. (b₁₋₄) As in Fig. 3a, but for AO.

greenhouse gases (Gillett et al., 2002) and the sea-ice-atmosphere feedback. Similar to AAO, models show quite poor capability to capture the interannual signal of AO.

5. Projections on future change of AAO and AO

Fyfe et al. (1999) showed positive trends of AO

and AAO indices during 1900–2100 using only one coupled general circulation model. However, results of individual models have large uncertainty, which can be reduced to some extent through the multi-model ensemble. The time series of multi-model-ensemble AAO index during 1970–2099 are shown in Fig. 6a. Significant trends exist in all four seasons, and MME-ozone and MME-nozone show equally significant positive trend. AAO shows a growing trend over the whole

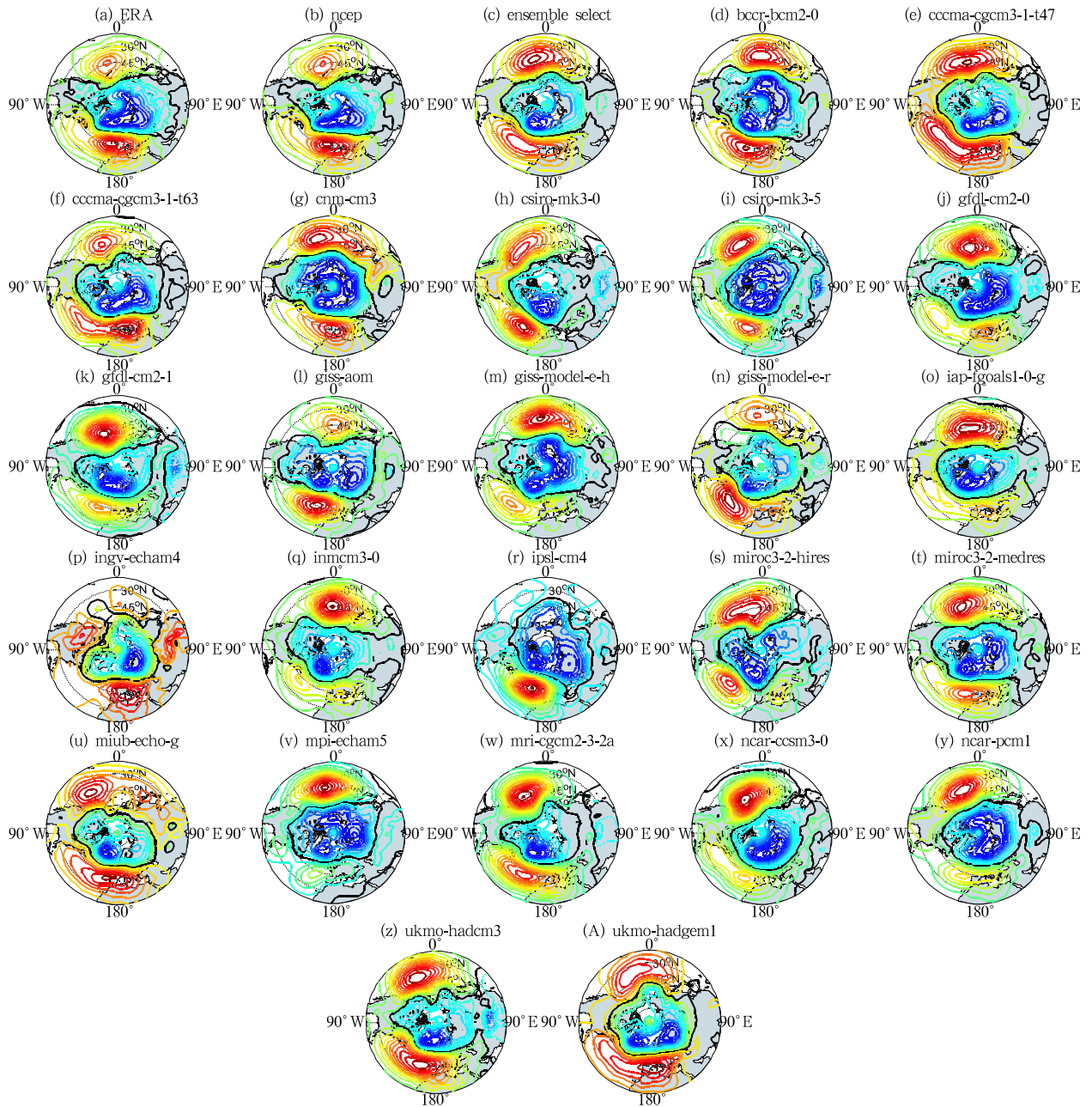


Fig. 5. As in Fig. 2, but for AO.

period, with decreasing SLP over the Antarctica and increasing SLP over midlatitude oceans. We compute the winter trend of every 30-yr during 1970–2089, and find that the significant increase occurs during 1970–1999 and 2060–2089, and the insignificant one during 2000–2029 and 2030–2059. Wavelet analysis of detrended MME winter AAO index shows a significant 16-yr period during 2000–2035 (figure omitted).

MME also shows a significant positive trend in AO index in all four seasons during 1970–2099 (Fig. 6b), and the summer trend has the least magnitude. AO index exhibits a steadier increase during the whole period relative to AAO.

In order to visualize the future change of SLP in polar regions, we compute the SLP difference between 1970–1999 and 2060–2089 based on the ensemble



Fig. 6. AAO (a) and AO (b) index during 1970-2099. Red, yellow, and green lines represent MME, MME-ozone, and MME-nozone, respectively.

average of the above selected models (Fig. 7). In the Northern Hemisphere, negative SLP anomalies appear in the polar region with three centers near the Bering

Strait, Barents Sea, and Hudson Bay, and values exceeding 2 hPa. Positive anomalies occupy the west and east coasts of the Pacific Ocean and the

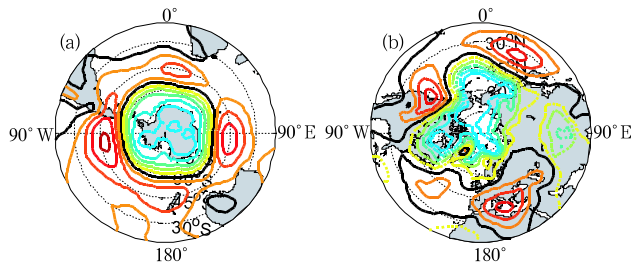


Fig. 7. Spatial difference of the SLP between 2060–2089 and 1970–1999 in the (a) Southern Hemisphere and (b) Northern Hemisphere in the ensemble mean of selected models. Contour interval is 30 Pa. Black thick contour denotes zero.

Mediterranean, manifesting that the Pacific center of AO will become weaker and expanded, and the positive center over the west coast of North America will get strengthened in 2060–2089. These changes may indicate the strengthening of AO in the Atlantic and the weakening in the Pacific Ocean, which will cause more asymmetry in the AO pattern. The SLP change in the Southern Hemisphere seems more zonally symmetric: the SLP in the polar region decreases consistently with a maximum of 1.5 hPa, and that in the midlatitude increases, manifesting the strengthened AAO in 2060–2089 compared with 1970–1999.

6. Summary

Twenty-four coupled models are succinctly evaluated in terms of the spatial structure and time series of AAO and AO, and their future changes are also briefly investigated. Models show large discrepancies in reproducing AO/AAO. Some models can capture the main spatial features of AAO, such as bccr-bcm2.0, cnrm-cm3, giss-model-e-h, giss-model-e-r, iap-fgoals1.0-g, miroc3.2-hires, mri-cgcm2.3.2a, ukmo-hadcm3, and ukmo-hadgem1; while some simulate AO better, e. g., cccma_cgcm_3.1_t47, cccma_cgcm_3.1_t63, gfdl_cm_2.0, giss-aom, miroc3.2-medres, ncar-pcm1, ukmo-hadcm3, and ukmo-hadgem1.

Simple all-model-ensemble cannot improve models' performance. The ensemble mean of the selected models after evaluation of individual models is an

effective way to obtain better results. Models' reproducibility is seasonally dependent, with best performance in winter. Most models simulate AAO better than AO, possibly due to the different topography. The South Polar region is occupied by the Antarctic continent, while the North Polar region by alternative land and sea, which induces more complicated atmospheric circulation field. The zonal asymmetry of AO also poses an obstacle to the models. On the other hand, the stratosphere ozone depletion contributes much to the positive trend of AAO, while for the AO trend, the ozone depletion is not a major factor, and the greenhouse gases and the albedo-sea ice feedback contribute much more, which makes the causes more complex (Arbalster et al., 2006). In addition, models basically cannot reproduce the internal variability of the climate system.

AO/AAO index keeps increasing during 1970–2099. AAO index shows a stronger upward trend than AO. The trend of AAO index changes over time, with the largest trend during 1970–1999 and 2060–2089, and insignificant during 2000–2029 and 2030–2059. In the SLP difference field between 2060–2089 and 1970–1999, obvious negative anomalies appear over both polar regions, and positive anomalies over midlatitude oceans, manifesting that AO/AAO will keep strengthening under the global warming. The ozone recovery may not exert significant influences on this trend.

In the polar regions, the stratosphere-troposphere coupling is an important dynamical process. The stratosphere polar vortex is critical to drive the tropospheric climate variability, and may be treated as a predictor for the tropospheric weather (Baldwin and Dunkerton, 2001; Thompson et al., 2005). We do analyze the polar vortex in the coupled models in the present study. However, primary results show that the corresponding stratospheric mode of AO/AAO in the models exhibits more differences than in the observation. In the reanalysis, the stratosphere over the South Polar (midlatitude) region is dominated by negative (positive) geopotential height anomalies, but the coupled models only show exaggerated signals over the polar region; for the Northern Hemisphere, coupled models can only reproduce half the amplitude

of the anomalies. According to these coarse results, it may be deduced that the coupled models probably cannot capture the stratosphere-troposphere interaction (Xin et al., 2008).

REFERENCES

- Arblaster, J. M., and G. A. Meehl, 2006: Contributions of external forcings to southern annular mode trends. *J. Climate*, **19**, 2896–2905.
- Baldwin, M. P., and T. J. Dunkerton, 2001: Stratospheric Harbingers of anomalous weather regimes. *Science*, **294**, 581–584.
- Boer, G. J., S. Fourest, and B. Yu, 2001: The signature of the annular modes in the moisture budget. *J. Climate*, **14**, 3655–3665.
- Cai, W., and T. Cowan, 2007: Trends in Southern Hemisphere circulation in IPCC AR4 models over 1950–99: Ozone depletion versus greenhouse forcing. *J. Climate*, **20**, 681–693.
- Fan, K., and H. Wang, 2006: Interannual variability of Antarctic Oscillation and its influence on East Asian climate during boreal winter and spring. *Science in China (series D)*, **49**, 554–560.
- Fyfe, J. C., G. J. Boer, and G. M. Flato, 1999: Arctic and Antarctic oscillations and their projected changes under global warming. *Geophys. Res. Lett.*, **26**, 1601–1604.
- Gillett, N. P., M. R. Allen, and K. D. Williams, 2002: The role of stratospheric resolution in simulating the Arctic oscillation response to greenhouse gases. *Geophys. Res. Lett.*, **29**, 138–138.
- , T. D. Kell, and P. D. Jones, 2006: Regional climate impacts of the Southern Annular Mode. *Geophys. Res. Lett.*, **33**, L23704.
- Gong Daoyi, 1998: Antarctic Oscillation. *Chinese Science Bulletin*, **13**, 296–301.
- , and C. Ho, 2003: Arctic oscillation signals in the East Asian summer monsoon. *J. Geophys. Res.*, **108**, 1–7.
- , Wang Shaowu, and Zhu Jinhong, 2001: East Asian winter monsoon and Arctic Oscillation. *Geophys. Res. Lett.*, **28**, 2073–2076.
- Hu, A., C. Rooth, R. Bleck, and C. Deser, 2002: NAO influence on sea ice extent in the Eurasian coastal region. *Geophys. Res. Lett.*, **29**, 10–11.
- Lorenz, D. J., and D. L. Hartmann, 2001: Eddy-Zonal Flow Feedback in the Southern Hemisphere. *J. Atmos. Sci.*, **58**, 3312–3327.
- , and —, 2003: Eddy-zonal flow feedback in the Northern Hemisphere winter. *J. Climate*, **16**, 1212–1227.
- Marshall, G. J., 2003: Trends in the Southern annular mode from observations and reanalyses. *J. Climate*, **16**, 4134–4143.
- , 2007: Half-century seasonal relationships between the Southern Annular mode and Antarctic temperatures. *Int. J. Climate*, **27**, 373–383.
- McHugh, M. J., and J. C. Rogers, 2001: North Atlantic oscillation influence on precipitation variability around the Southeast African convergence zone. *J. Climate*, **14**, 3631–3642.
- Moritz, R. E., C. M. Bitz, and E. J. Steig, 2002: Dynamics of recent climate change in the Arctic. *Science*, **297**, 1497–1502.
- Raphael, M. N., and M. M. Holland, 2006: Twentieth century simulation of the southern hemisphere climate in coupled models. Part I: Large scale circulation variability. *Climate Dyn.*, **26**, 217–228.
- Rigor, I. G., J. M. Wallace, and R. L. Colony, 2002: Response of sea ice to the Arctic oscillation. *J. Climate*, **15**, 2648–2663.
- Taylor, K. E., 2001: Summarizing multiple aspects of model performance in a single diagram. *J. Geophys. Res.*, **106**, 7183–7192.
- Thompson, D. W. J., and J. M. Wallace, 1998: The Arctic Oscillation signature in the wintertime geopotential height and temperature fields. *Geophys. Res. Lett.*, **25**, 1297–1300.
- , and —, 2000a: Annular modes in the extratropical circulation. Part I: Month-to-month variability. *J. Climate*, **13**, 1000–1016.
- , and —, 2001: Regional climate impacts of the Northern Hemisphere annular mode. *Science*, **293**, 85–89.
- , and S. Solomon, 2002: Interpretation of recent Southern Hemisphere climate change. *Science*, **296**, 895–899.
- , J. M. Wallace, and G. C. Hegerl, 2000b: Annular Modes in the Extratropical Circulation. Part II: Trends. *J. Climate*, **13**, 1018–1036.
- , M. P. Baldwin, and S. Solomon, 2005: Stratosphere-troposphere coupling in the Southern Hemisphere. *J. Atmos. Sci.*, **62**, 708–715.
- Wang Huijun and Fan Ke, 2005: Central-north China precipitation as reconstructed from the Qing dynasty: Signal of the Antarctic atmospheric oscillation. *Geophys. Res. Lett.*, **32**, L24705.
- Xin Xiaoge, Zhou Tianjun, and Yu Rucong, 2008: The Arctic Oscillation in coupled climate models. *Chinese J. Geophys.*, **51**, 337–351. (in Chinese)